Observational constraints on the dynamics of the interplanetary magnetic field dissipation range

Robert J. Leamon, Charles W. Smith, Norman F. Ness,
and William H. Matthaeus

Bartol Research Institute, University of Delaware, Newark

Hung K. Wong

Aurora Science Inc., San Antonio, Texas

Abstract. The dissipation range for interplanetary magnetic field fluctuations is formed by those fluctuations with spatial scales comparable to the gyroradius or ion inertial length of a thermal ion. It is reasonable to assume that the dissipation range represents the final fate of magnetic energy that is transferred from the largest spatial scales via nonlinear processes until kinetic coupling with the background plasma removes the energy from the spectrum and heats the background distribution. Typically, the dissipation range at 1 AU sets in at spacecraft frame frequencies of a few tenths of a hertz. It is characterized by a steepening of the power spectrum and often demonstrates a bias of the polarization or magnetic helicity spectrum. We examine Wind observations of inertial and dissipation range spectra in an attempt to better understand the processes that form the dissipation range and how these processes depend on the ambient solar wind parameters (interplanetary magnetic field intensity, ambient proton density and temperature, etc.). We focus on stationary intervals with well-defined inertial and dissipation range spectra. Our analysis shows that parallel-propagating waves, such as Alfvén waves, are inconsistent with the data. MHD turbulence consisting of a partly slab and partly two-dimensional (2-D) composite geometry is consistent with the observations, while thermal particle interactions with the 2-D component may be responsible for the formation of the dissipation range. Kinetic Alfvén waves propagating at large angles to the background magnetic field are also consistent with the observations and may form some portion of the 2-D turbulence component.

1. Introduction

Two paradigms are currently in vogue for describing the basic nature of low-frequency (from $< 10^{-4}$ to ~ 1 Hz in the spacecraft frame), interplanetary magnetic field (IMF) fluctuations. In the first paradigm, IMF fluctuations are thought to consist mostly of waves derivable from the magnetohydrodynamic (MHD) equations (see *Coleman* [1966] and review by *Barnes* [1979]). The traditional argument holds that

these waves originate at the Sun near the Alfvén critical point, propagate outward, and are largely unaffected along the propagation path except for WKB transport effects [see *Hollweg*, 1990]. The near-Sun source is supported in part by observations near 1 AU of correlations between the magnetic and fluid velocity fluctuations that suggest a predominantly outward propagation of the wave [*Belcher and Davis*, 1971]. Propagation of the waves parallel to the am-

bient mean magnetic field is commonly assumed on the basis of the observation of minimum variance directions that tend to be aligned with the mean field near 1 AU [*Belcher and Davis*, 1971; *Daily*, 1973].

Apart from the high IMF-fluid velocity correlations (high cross helicity) several other observations and theoretical considerations support and refine the wave paradigm. The damping of slow mode waves generally and of the fast mode wave due to nonlinear steepening and Landau damping at nonzero angles of propagation relative to the mean magnetic field suggest that the parallel-propagating Alfvén mode should be dominant in the solar wind. Such waves, with limited nonlinear interactions, may be a remnant signature of solar atmospheric fluctuations if the wave paradigm is correct.

In the second paradigm, the turbulence paradigm, it is argued that the IMF fluctuations are fundamentally nonlinear and interactive so that self-organization of fluctuations over a broad range of frequencies is accomplished [*Coleman*, 1968; *Matthaeus and Goldstein*, 1982]. In this model, fluctuation energy that originates at or near the sun may propagate or convect outward, but added energy due to large-scale, in situ processes and dissipation may be important [*Goldstein et al.*, 1995; *Tu and Marsch*, 1995]. The magnetic energy is transferred through the spectrum to spatial scales that might otherwise be depleted so that a self-deterministic spectrum is achieved. In this paradigm the IMF fluctuations in the range from $< 10^{-4}$ to ~ 1 Hz form the "inertial range" of the spectrum, and heating is implied [*Coleman*, 1968].

There is now ample evidence that both the inner heliosphere [*Freeman*, 1988; *Marsch*, 1991] and the outer heliosphere [*Richardson et al.*, 1995] are subject to a measurable degree of in situ heating. While shock compression may provide a measure of that heating [*Zank et al.*, 1996] the dissipation of IMF fluctuations has been argued to provide a means for the majority of the heating of the solar wind in the inner heliosphere [*Coleman*, 1968].

If dissipation of magnetic energy is needed to account for the apparent heating of the solar wind plasma, then the above two paradigms imply potentially very different heating rates. If the IMF fluctuations are noninteracting waves, then the wave energy at a given frequency (asssumed to be significantly lower than the cyclotron frequency) is unavailable for heating the background ions until the kinetic processes responsible for coupling the fluctuations to the background ions are shifted to that given frequency through changes in the background parameters [cf. *Schwartz et al.*, 1981, Figure 1]. For instance, the

cyclotron frequency, where resonant dissipation becomes significant for Alfvén waves, scales with the mean magnetic field, $\Omega_{ci} \sim B$, so the cyclotron frequency varies with heliocentric distance as $\Omega_{ci} \sim R^{-1}$ in the outer heliosphere. Within the inner heliosphere, $\Omega_{ci} \sim R^{-2}$. This suggests a relatively slow process whereby the IMF fluctuation spectrum is consumed from the high-frequency end only as the kinetic processes of wave damping shift to lower frequency. This greatly limits the amount of energy available for in situ heating of the background ions and has been shown by *Schwartz et al.* [1981] to be inadequate to explain the apparent heating of thermal ions in high-speed streams. Consideration of minor ion species permits cyclotron damping at lower frequencies, but only at reduced rates, because of the reduced number density.

Other damping mechanisms, such as Landau damping [*Barnes*, 1966, 1979; *Stix*, 1992], operate over a wide range of wave frequencies. As such, it is unclear whether or how they would lead to a sharp spectral feature of the type we discuss here. We adopt the implication, taken from traditional fluid dynamics, that a spectral break at the high-frequency end of the inertial range leading to a steepened power spectrum is indicative of the onset of dissipation. Other interpretations are not ruled out by this analysis.

If the IMF fluctuations are fundamentally turbulent with a self-organizing spectrum and active spectral cascade of energy from large spatial scales to small scales, then the so-called "energy-containing fluctuations" at the largest spatial scales [*Batchelor*, 1953] provide a source of energy which is transferred through the inertial range to replenish the depleted high-frequency spectrum and thereby enhance the heating of the background ions. Indeed, such an energy-containing spectral transfer is the very definition of an inertial range [*Kolmogoroff*, 1941]. The high-frequency region of the spectrum where magnetic energy is coupled to the thermal motions of the ions is known in traditional fluid turbulence theory as the dissipation range [*Batchelor*, 1953], and it is characterized by a steepening of the power spectrum relative to the inertial range such as is seen in the solar wind at frequencies comparable to the proton gyroradius [*Behannon*, 1975; *Denskat et al.*, 1983; *Smith et al.*, 1990; *Goldstein et al.*, 1994]. In this way, IMF turbulence may provide an enhanced heating rate relative to the wave paradigm so long as (1) an active spectral transfer of magnetic energy is maintained to replenish the damped oscillations and (2) a mechanism is available for coupling the magnetic fluctuations of the dissipation range to the background ions.

Whatever the dynamic nature of the fluctuations may be and however the magnetic spectrum may evolve in the solar wind, we can test some aspects of the models for the dissipation dynamics as well as the geometry of the magnetic spectrum using in situ measurements. By geometry we mean the relative distribution of energy over the full three-dimensional (3-D) space of wave vectors. By dissipation dynamics we consider here whether simple models of cyclotron damping by parallel-propagating Alfvén waves can provide sufficient organization of the observations to warrant refined treatments.

To this end, we examine IMF fluctuations within the dissipation range using Wind data collected at 1 AU. In section 2 we describe our method for characterizing the dissipation range fluctuations and present the basic parameterization of the intervals used in this study. In section 3 we apply these observations to the parallel-propagating wave model for IMF fluctuations and conclude that such waves are unable to account for the observed characteristics of the data set. In section 4 we analyze the geometry of the dissipation range and find that a large fraction of the total power resides in wave vectors that are quasi-perpendicular to the mean magnetic field. In section 5 we discuss how obliquely propagating waves might form the dissipation range, and in section 6 summarize our findings.

Throughout the paper we use the language of parallel-propagating and obliquely propagating plasma waves together with that of MHD turbulence theory. No distinction regarding the dynamics of spectral evolution is intended unless explicitly stated. In section 5 we embrace both concepts and allow for the possibility that kinetic Alfvén waves may form a significant component of the turbulence. We conclude that parallel-propagating Alfvén waves form only a minority component of the total spectrum.

2. The Wind Data Set

This study uses 33 one-hour intervals of magnetic field data from the Wind Magnetic Field Investigation (MFI) instrument [Lepping et al., 1995] and thermal particle measurements from the SWE instrument [Ogilvie et al., 1995] recorded in the solar wind when in near-Earth orbit between January 1995 and February 1997. Wind was typically between 100 R_E and 200 R_E upstream during the intervals in question. For all intervals in this study we use the highest available resolution magnetic field data; depending on the distance from Wind to Earth, the sampling rate was either 46, 92, or 184 ms. The resolution of the plasma data was 92 s.

No attempt was made to limit this study to "...the purest examples of ... outwardly propagating Alfvén waves occur[ring] in high-velocity solar wind streams and on their trailing edges..." as did *Belcher and Davis* [1971, p. 3534] or to exclude disturbance regions such as coronal mass ejections or shocked plasma. We do attempt to eliminate periods of non-stationary behavior that might lead to improperly computed spectra, and intervals with power spectra that demonstrate significant upstream wave activity (due to apparent magnetic connection to the Earth's bow shock) are also rejected. Some spectra computed were rejected because no break in the spectrum was visible below the Nyquist frequency. Only periods that result in power law inertial range spectra are kept; power law dissipation range spectra were virtually always seen when a distinct spectral break was observed, and it was generally a poorly determined inertial range spectrum that led to the rejection of some candidate intervals in this study. This study makes no claim of applicability outside this limitation.

The 33 intervals used here span a wide range of basic plasma parameters:

$$333 \le V_{SW} \le 692 \text{ km s}^{-1}$$
$$3.1 \le \langle B \rangle \le 28.5 \text{ nT}$$
$$9.1° \le \Theta_{BV_{SW}} \le 87.1°$$
$$0.034 \le \beta_p \le 2.75$$
$$18.5 \le v_A \le 110.2 \text{ km s}^{-1}$$
$$2.3 \le n_p \le 49.5 \text{ cm}^{-3}$$
$$2.24 \times 10^4 \le T_p \le 4.09 \times 10^5 \text{ K},$$

which are solar wind speed, magnetic field strength, field-to-flow angle, proton plasma β, Alfvén speed, proton density, and proton temperature, respectively.

The cross correlation between magnetic field and solar wind velocity fluctuations,

$$\sigma_{BV} \equiv \langle \delta \mathbf{v_A} \cdot \delta \mathbf{V} / (|\delta \mathbf{v_A}||\delta \mathbf{V}|) \rangle \qquad (1)$$

where $\delta \mathbf{v_A} \equiv \delta \mathbf{B} / \sqrt{\mu_0 n_p m_p}$, was computed using 92 s data. The cross correlation σ_{BV} differs from the cross helicity but is similarly constrained to be $-1 \le \sigma_{BV} \le +1$. It provides an indication of the relative percentage of sunward and antisunward propagating Alfvén waves in the inertial range. Seven of the 33 periods studied showed a dominance of sunward propagating waves with three of these seven having $|\sigma_{BV}| \le 0.25$.

Figure 1 shows the trace of the power spectral density matrix for hour 1300 on day 30 of 1995, which is typical in most regards of the events used here. The high-frequency end of the inertial range spectrum is
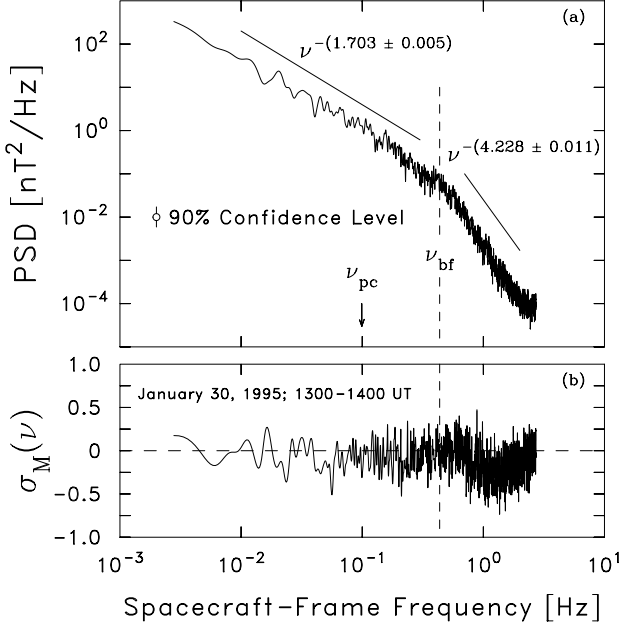
Figure 1. Typical interplanetary power spectrum showing the inertial and dissipation ranges. (a) Trace of the spectral matrix with a break at $\sim$0.4 Hz where the dissipation range sets in. (b) The corresponding magnetic helicity spectrum. The date and time of the data used are given.

shown at spacecraft frame frequencies $\nu_{sc} < 0.44$ Hz. The inertial range terminates in a spectral break to a steeper spectral index. This spectral break marks the onset of the dissipation range at $\nu_{sc} > 0.44$ Hz. We return to Figure 1 below in sections 2.1 and 2.2.

2.1. Method

We used the following algorithm to analyze each data interval:

1. Eliminate "flyers" and bad points. Any measurement that is more than 3.5σ from the mean in any component is removed. Typically, 1% of the data set ($\sim$400 points out of 40,000) are removed in this way. The gaps so created are linearly interpolated.

2. Prewhiten the data with a first-order difference filter to reduce the influence of leakage when computing the spectra.

3. Compute the power spectra using the correlation matrix method of *Blackman and Tukey* [1958]. A maximum lag of 10% of the length of the data set results in 20 degrees of freedom for the spectral estimates. The resulting spectra are then postdarkened

to correct for the earlier prewhitening [*Chen*, 1989; *Bieber et al.*, 1993].

4. Fit power laws to inertial and dissipation range spectra using a least squares fit. We omit frequencies close to the apparent spectral breakpoint when fitting the two spectral ranges. Figure 1 is typical in most respects of the spectra considered here, except in that it does not show sharp peaks at harmonics of the spacecraft spin tone. However, these are an almost omnipresent feature in spectra with slightly lower power levels. Consequently, these frequencies (harmonics of 0.33 Hz) are omitted from the least-squares fitting of the two ranges using a $\pm 10\%$ window around each harmonic. A flattening of the high-frequency spectrum is evident in Figure 1 at frequencies > 1 Hz and is more evident in other intervals with lower power levels and higher Nyquist frequencies. The flattened spectrum is not associated with the IMF, and the source of this noise is under investigation by the MFI team. We omit the flattened spectra from the spectral fitting. From the intersection of the two power law fits we can calculate the breakpoint frequency for the onset of dissipation.

On average, the uncertainty in the spectral breakpoint frequency produced by this method is 21% of the computed spectral breakpoint frequency.

2.2. Preliminary Results

Figure 1 shows the computed spectral fits derived from the above analysis for the hour in question. The computed spectral breakpoint frequency is $\nu_{bf} = 0.44$ Hz and the fitted inertial and dissipation range spectra are $\nu^{-(1.703\pm0.005)}$ and $\nu^{-(4.228\pm0.011)}$, respectively. The fitted inertial range spectra for the 33 events range from $\nu^{-(1.46\pm0.01)}$ to $\nu^{-(1.93\pm0.02)}$. The average fit of inertial range spectra is $\nu^{-1.66}$, in excellent agreement with the $\nu^{-5/3}$ prediction of *Kolmogoroff* [1941]. The dissipation range spectra range from $\nu^{-(2.00\pm0.02)}$ to $\nu^{-(4.43\pm0.01)}$, with the average being $\nu^{-3.04}$. No clear correlation between the fitted indices of the two ranges is observed.

Figure 1b shows the reduced magnetic helicity spectrum for that interval. Magnetic helicity is constrained to be $-1 \leq \sigma_M(\nu) \leq +1$ and is a measure of the spatial handedness of the magnetic field [*Moffatt*, 1978]. It can be related to the polarization in the plasma frame if the propagation direction is known [*Smith et al.*, 1983]. There is a negative signature at dissipation range frequencies, averaging -0.275 over those frequencies used to calculate the dissipation range spectral slope. The majority of intervals have helicity signatures: 13 out of 33 have $|\sigma_M| > 0.2$; 21 out of 33 have $|\sigma_M| > 0.15$; and 27 out
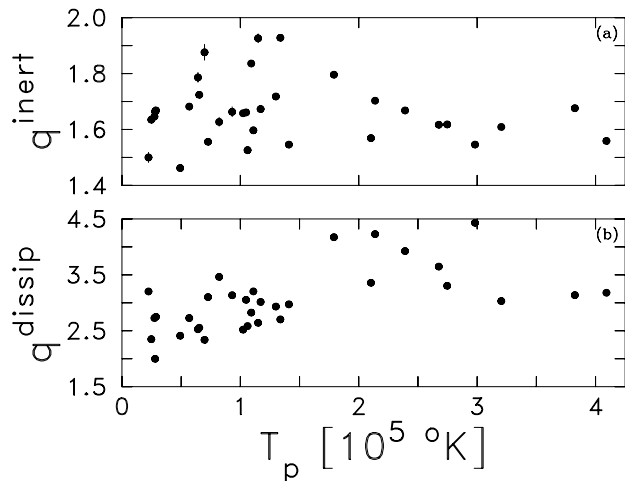
Figure 2. (a) Dependence of inertial range spectral index and (b) dissipation range spectral index on solar wind proton temperature. There are error bars on this plot; on only four of the points do the error bars exceed the size of the bullet.

of 33 have $|\sigma_M| > 0.1$. *Goldstein et al.* [1994] noted similar behavior wherein many, but not all, intervals studied by them showed significant magnetic helicity signatures in the dissipation range. We will return to this result in section 3.

The *Belcher and Davis* [1971, p. 3534] examination of inertial range frequencies argues that "the spectra with slower falloffs tend to be associated with higher temperature regions," and we observe this same dependence at a statistical level (see Figure 2a). However, it is perhaps more correct to state that the range of inertial range indices narrows with increasing proton temperature and concentrates on the lowest values in the observed range. The dissipation range indices computed in this analysis behave in the opposite sense: high-temperature proton distributions tend to show the steepest spectra (see Figure 2b). This suggests that steeper dissipation range spectra imply greater heating rates.

The cyclotron frequency computed from the average magnitude of the field for the interval shown in Figure 1 is $\nu_{pc} = 0.099$ Hz. It is always the case for the 33 periods examined that $\nu_{pc} < \nu_{bf}$ as shown in Figure 3, but it is also the case that $\nu_{pc} > 0.1\nu_{bf}$. We will return to this in section 3.

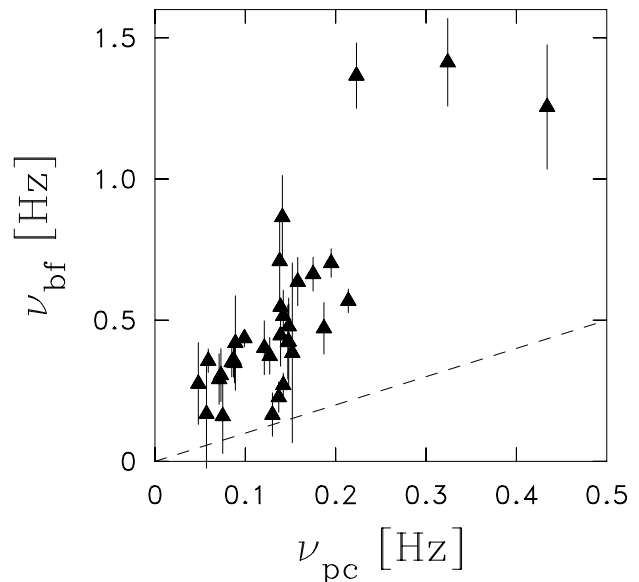### 2.3. Transverse Fluctuations

Belcher and Davis [1971] demonstrate that the in-

Figure 3. Behavior of the observed break frequency ν_{bf} versus proton cyclotron frequency ν_{pc}. As cyclotron frequency scales with B, the behavior of break frequency with IMF strength is also shown. The dashed curve corresponds to equality $\nu_{bf} = \nu_{pc}$.

ertial range fluctuations $1.6 \times 10^{-4} < \nu_{sc} < 0.04$ Hz are largely transverse to the mean magnetic field. They define a coordinate system relative to the mean magnetic field direction $\hat{\mathbf{B}}$ and radial direction $\hat{\mathbf{R}}$ according to $(\hat{\mathbf{B}} \times \hat{\mathbf{R}}, \hat{\mathbf{B}} \times (\hat{\mathbf{B}} \times \hat{\mathbf{R}}), \hat{\mathbf{B}})$ and conclude that the average variances for these three components have the ratio 5:4:1. *Klein et al.* [1991] and *Chen et al.* [1991] have subsequently shown variations in this result. We note that this implies a ratio for the total variance transverse to and aligned with the mean field of 9:1. We extend this analysis for inertial range frequencies $0.01 \lesssim \nu_{sc} \lesssim 0.3$ Hz and dissipation range frequencies $0.5 \lesssim \nu_{sc} \lesssim 1.5$ Hz (with large variation due to the location of the computed spectral breakpoint).

We define $P_{\parallel}$ to be the power in fluctuations parallel to $\hat{\mathbf{B}}$ and $P_{\perp}$ to be the total power in both components perpendicular to the mean field. Therefore $P_{\perp} + P_{\parallel}$ is the total power (trace of the spectral matrix) which is plotted in Figure 1. We acknowledge the difference between our method using spectral power and that of *Belcher and Davis* [1971], who use average variances.

For the high-frequency end of the inertial range our results find a mean $P_{\perp}:P_{\parallel}$ ratio of 14:1, with a
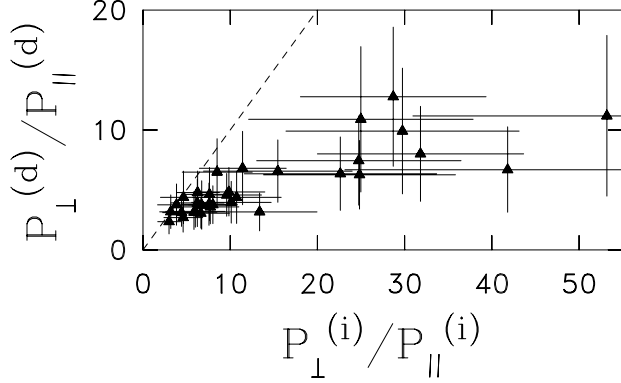
Figure 4. Ratio $P_\perp/P_\parallel$ for the inertial (superscript "(i)") and dissipation (superscript "(d)") ranges. The dashed curve again represents equality.

Figure 5. Dispersion relations based on numerical solutions of the linearized Vlasov-Maxwell equations. The real part of the frequency, ω_r, is given by the solid curve and left-hand scale. The imaginary part, or decay rate, γ, is given by the dashed curve and right-hand scale. The top two curves for ω_r and γ give the solution for $\beta = 0.1$ and the bottom two curves give the solution for $\beta = 1.0$.

range $3.0 \leq P_\perp/P_\parallel \leq 53.2$. Taking into account that the above arithmetic mean may be unduly biased by several samples with unusually large values, we note that the geometric mean of $P_\perp/P_\parallel$ is only 10.4, which is in closer agreement with the result of *Belcher and Davis* [1971]. For the dissipation range we find a mean ratio of 5.4:1 with a range of $2.36 \leq P_\perp/P_\parallel \leq 12.8$ and a geometric mean ratio of 4.9:1. A comparison of the ratios of transverse to parallel power for the two spectral ranges is shown in Figure 4. The dissipation range ratios $P_\perp/P_\parallel$ are consistently less than inertial range ratios, implying a decreased importance of transverse fluctuations in the dissipation range and a relative increase in the compression of the plasma at these scales.

3. Parallel-Propagating Waves

In section 2 we noted that most, but not all, dissipation range spectra have moderate bias of the magnetic helicity. Again using our exemplary period, we note that $\langle B_R \rangle = -4.9$ nT and $\text{sign}(\langle B_R \rangle)\langle \sigma_M \rangle > 0$, which implies either a predominance of outward propagating, right-hand polarized waves or inward propagating, left-hand polarized waves [*Smith et al.*, 1983]. If we repeat this same analysis for all 33 periods in this study, we find that only six intervals have $\text{sign}(\langle B_R \rangle)\langle \sigma_M \rangle < 0$, in contrast to the above example. We are unable to infer the propagation direction for dissipation range fluctuations bacause of the time resolution of the plasma data. If we compare the magnetic helicity in the dissipation range with the cross correlation σ_{BV} in the inertial range and assume that the dissipation range cross correlation is the same as
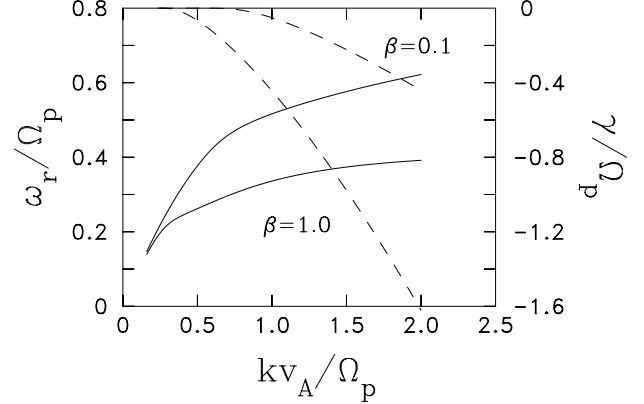
for the inertial range, then we find that only three of the 33 intervals studied have magnetic helicity signatures that are inconsistent with ion cyclotron damping of Alfvén waves [*Stix*, 1992]. Such periods could be consistent with ion cyclotron damping if $\beta_p \gg 1$, which would alter the range of polarizations that provide resonance with thermal ions, but in the three cases here, $\beta_p = 0.034$, 0.191, and 0.885. We find no unique features to otherwise segregate these three intervals as atypical of the set. The magnetic helicity and cross-correlation analyses suggest that the dissipation range is generally consistent with the depletion of Alfvén waves.

Several damping mechanisms can readily be considered for the formation of the dissipation range (see *Barnes* [1979] for a discussion of several, including Landau damping). The apparent depletion of outward propagating Alfvén waves at frequencies comparable to the proton cyclotron frequency (Figure 1b) naturally suggests resonant cyclotron damping of Alfvén waves as a leading candidate, as first suggested by *Coleman* [1968]. We pursue this suggestion with a series of tests which use the cyclotron damping mechanism in an attempt to predict the onset of the dissipation range.

3.1. Cyclotron-Resonant Wave Damping

For frequencies $\omega_r \ll \Omega_p$, where ω_r is the plasma-frame wave frequency and Ω_p is the proton cyclotron frequency, the dispersion relation for left-hand polarized Alfvén-ion cyclotron waves, hereafter Alfvén waves, propagating parallel to the magnetic field is [*Stix*, 1992]

$$\omega_r = k_\parallel v_A, \tag{2}$$

where $k_\parallel = \mathbf{k} \cdot \hat{\mathbf{B}}$ is the wavenumber component parallel to the ambient magnetic field and v_A, the Alfvén velocity, is given by

$$v_A = c \frac{\Omega_p}{\omega_{pi}} = \frac{B}{\sqrt{\mu_0 n_p m_p}}. \tag{3}$$

For higher frequencies, dissipation becomes important and the solution becomes dispersive. Figure 5 shows two solutions to the linearized Vlasov-Maxwell equations for two values of $\beta = v_{th}^2 / v_A^2$ that extend into the range where dissipation becomes significant. We assume single-temperature Maxwellian distributions for both protons and electrons with $T_p = T_e$. The solutions for ω_r approach Ω_p asymptotically as dissipation increases. Dissipation sets in at lower wavenumbers for hotter distributions (increased β) so that the onset of dissipation becomes dependent upon the proton temperature.

The resonance condition for cyclotron damping in the plasma frame is

$$\omega_r - \mathbf{k} \cdot \mathbf{v} = \pm \Omega_p, \tag{4}$$

where $\mathbf{v}$ is the particle velocity. For outward propagating waves and inward moving ions we can reduce the resonance condition to a prediction for the minimum resonant wavenumber:

$$\omega_r + k_\parallel v_p = +\Omega_p, \tag{5}$$

where v_p is the proton speed.

The (Maxwellian) spread of particle speeds, v_{th}, results in a spread of wavenumbers that can resonate with the protons. We have two methods to calculate at which frequency dissipation should set in:

3.1.1. Simple slab calculation
We assume that $v_p = v_{th}$ and that damping sets in at $\omega_r = k v_A \ll \Omega_p$. Substituting this into the resonance condition (equation (5)) gives

$$k_d = \frac{\Omega_p}{v_A + v_{th}} \tag{6}$$

as an estimate for the minimum, outward propagating wavenumber at which dissipation by resonance with

the background ion distribution becomes important. In principle, if the dissipation range is made up of outward propagating Alfvén waves, then this estimate for k_d should determine the onset of the dissipation range. We can use Figure 5 as a rough check of the validity of the estimate of (6): when $\beta_p = 1$, $v_A = v_{th}$, and $k v_A / \Omega_p = \frac{1}{2}$. From Figure 5 we can see that this corresponds to $\gamma / \Omega_p \simeq -0.05$, so dissipation has started; however, combining $k v_A / \Omega_p = \frac{1}{2}$ with (2), we get $\omega_r / \Omega_p = \frac{1}{2}$, which is an overestimate. Following the second set of traces for $\beta_p = 0.1$ predicts $\omega_r / \Omega_p = k v_A / \Omega_p = 0.9$, which again gives reasonable dissipation rates of $\gamma / \Omega_p \simeq -0.05$ but overestimates ω_r.

Once we know the wavenumber at which dissipation starts, we may use the Doppler shift to compute the frequency of an (outward propagating) Alfvén wave resonant with a particle with the mean thermal speed:

$$\nu_{sc} = \frac{\mathbf{k} \cdot \mathbf{V}_{SW}}{2\pi} + \frac{\omega_r}{2\pi}. \tag{7}$$

It is possible to find a lower-frequency wave at which the same dissipation rate is present, but this would be an inward propagating solution. If present, the dissipation of this wave would be obscured by outward propagating waves at the same spacecraft frequency with less dissipation, so presumably they would retain greater energy. Either way, the conclusions are nearly equivalent.

3.1.2. Numerical solution calculation
Alternately, we can apply the numerical solutions of the type shown in Figure 5 and assume that the dissipation range begins when $|\gamma|$ is some fraction of ω_r; say, one third or one tenth. That is, we are considering departures from the dispersion relation of (2). We then take the the critical wavenumber k_d and wave frequency ω_r from the numerical solutions. We can again use (7) to translate to a spacecraft-frame frequency.

Since we are making the parallel-propagation assumption, that is, $\Theta_{BV_{SW}} = \theta_{kV_{SW}}$, the vector dot product in (7) implies a dependence on $\Theta_{BV_{SW}}$ for the dissipation onset frequency for both the numerical solution and slab calculation.

3.2. Results

Figure 6 shows two events that are almost identical in ambient parameters but with very different field-to-flow angles $\Theta_{BV_{SW}}$: 23° and 87°. Using the observed average plasma parameters ($\langle B \rangle = 6.4$ nT, $\beta_p = 0.71$, $V_{SW} = 692$ km s^{-1}, and $\Theta_{BV_{SW}} = 23°$), the prediction for the spectral breakpoint of the first
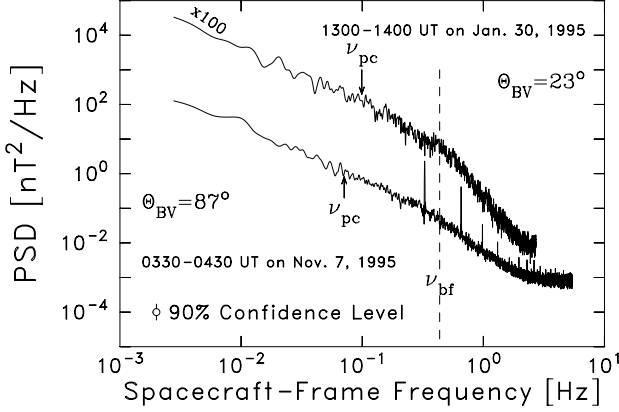
Figure 6. Two examples. The top curve is the same spectrum shown in Figure 1; the bottom curve is from November 7, 1995. The two intervals have similar $\langle B \rangle$, β, and V_{SW} but very different values of $\Theta_{BV_{SW}}$; the second example has an almost perpendicular magnetic field. The second interval is also from a time period when Wind was in its high-rate data mode: the sampling rate and thus Nyquist frequency are twice that of the earlier example. Spacecraft spin tone harmonics are evident in the bottom trace.

event (the top curve in Figure 6) using the simple slab calculation is 0.59 Hz. This is in relatively good agreement with the measured breakpoint value of 0.44 Hz. The average plasma parameters for the second event (the bottom curve in Figure 6) are $\langle B \rangle = 4.6$ nT, $\beta_p = 0.67$, $V_{SW} = 524$ km s^{-1}, and $\Theta_{BV_{SW}} = 87°$. From the $\mathbf{k} \cdot \mathbf{V}_{SW}$ term in (7) we expect the Doppler shift of the second event should be smaller by a factor of v_A/V_{SW}, and the observed spectral breakpoint should be ~1 decade lower in frequency in the spacecraft reference frame. The predicted spacecraft-frame frequency for the spectral breakpoint in this instance using the simple slab model is 0.08 Hz, which stands in contrast with the observed value of 0.29 Hz. The nearly identical frequencies marking the onset of the dissipation range for these two events contradict the expectations and the predictions of parallel-propagating, cyclotron-damped Alfvén wave theory.

These two events are not exceptions to the rule. Figure 7 compares the predicted spectral break frequencies derived from the three cyclotron resonance models above, ν_{th}, with the observed spectral breakpoint frequencies. Although all three models give order-of-magnitude agreement with the observations, none exhibits any close correlation with the observations. The models are unsatisfactory. This might only
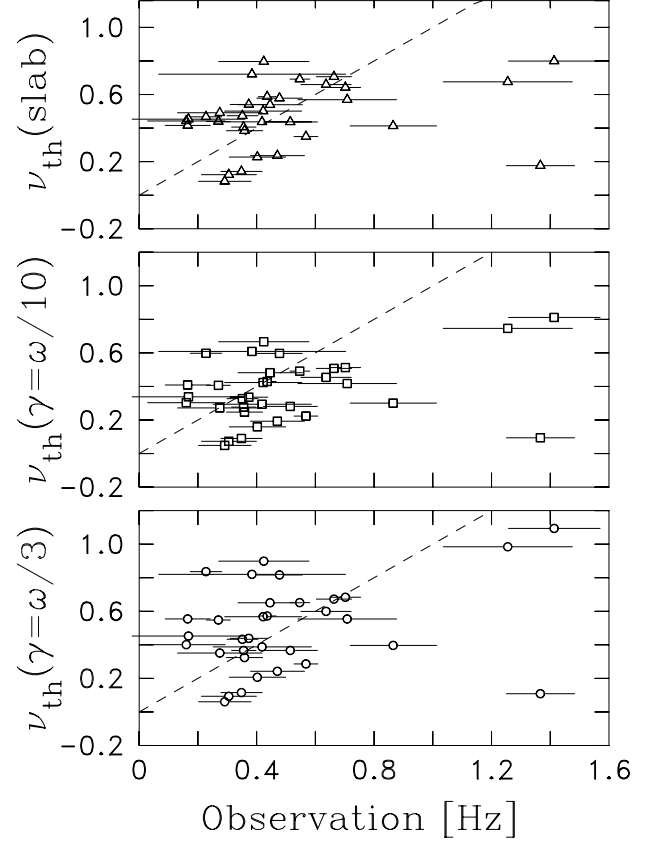

Figure 7. Comparison of observed spectral breakpoint frequency with predictions derived from (top) the simple slab model (triangles) and the numerical results for (middle) $|\gamma| = \omega_r/10$ (squares) and (bottom) $|\gamma| = \omega_r/3$ (circles). Dashed curves represent equality. Although the predictions are generally in order-of-magnitude agreement with the observations, the necessary linear scaling is not observed.

reflect the simplicity of these three models were it not for an underlying order in the results not evident in Figure 7.

The systematic error of the theories is revealed in Figure 8, where we plot the fractional error of the theory relative to the observation, $(\nu_{bf} - \nu_{theory})/\nu_{bf}$, for (1) the simple model (triangles); (2) the numerical solutions for $|\gamma| = \omega_r/10$ (squares); and (3) the numerical solutions for $|\gamma| = \omega_r/3$ (circles). All three theories exhibit a broad scatter of error where the theories tend to overestimate the observations for values of $\Theta_{BV_{SW}} < 50°$. The fractional error increases systematically for $\Theta_{BV_{SW}} > 50°$. To demonstrate that the observations are best fit by a theory of non-field-
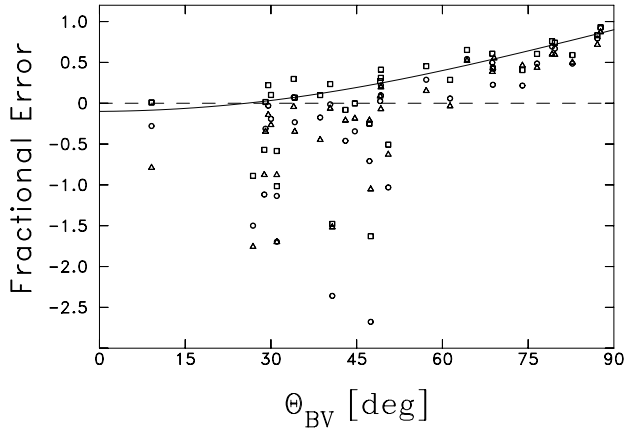
Figure 8. Fractional error for all three models discussed in the text as a function of field-to-flow angle. The symbols are the same as in Figure 7. The error is greatest at large angles, true for all wave formulations.

aligned wave vectors, the solid curve is derived from the Doppler shift condition under (1) the definition that $k_r \equiv 2\pi\nu_{\text{bf}}/V_{SW}$ is the breakpoint wavenumber measured along the (radial) solar wind direction and the assumptions that (2) the true wavenumber is aligned with the magnetic field, $k_\parallel = k_r/\cos(\Theta_{BV_{SW}})$ and (3) $\omega_r/(k_r V_{SW}) = 0.1$. This demonstrates that the imposition of a $\Theta_{BV_{SW}}$ dependence upon the observations leads to a systematic error in the results.

It is evident from the data and this analysis that any explanation of magnetic dissipation in the solar wind based on a slab-like, 1-D geometry is likely to lead to a contradiction with observations. We acknowledge that our treatment here, while employing a fully numerical solution of the dispersion relation, can be improved by considering numerous aspects of the plasma, including, for instance, multitemperature Maxwellian distributions. Even so, we contend that any wave mode thought to be associated with the damping process and that propagates at less than the solar wind speed will suffer from a systematic introduction of error if the wave vector is required to be field aligned. This can only be avoided if (1) a systematic correlation between $\Theta_{BV_{SW}}$ and some critical plasma parameter exists that fundamentally alters the resonant process for large $\Theta_{BV_{SW}}$ or (2) the geometry of the magnetic fluctuations is greater than one dimensional. In the remainder of this paper we pursue this latter possibility.

4. Quasi-2-D (Oblique) Wave Vectors

In section 2.3 we considered the spectrum of fluctuations in a field-aligned coordinate system and found that the ratio of power in the two perpendicular directions to the parallel direction decreased in the dissipation range with respect to the inertial range (Figure 4). Following *Bieber et al.* [1996], in a test based on the analysis of *Oughton* [1993], we can use the ratio of the power in the two perpendicular directions as another test of the geometry of the fluctuations.

Let us define a right-handed orthogonal coordinate system in which the z axis is aligned with the mean magnetic field and points away from the Sun, the x axis is in the plane defined by the mean field and the solar wind velocity vector (assumed to be radial) and also points away from the Sun, and the y axis completes the right-handed system. This is the $(\hat{\mathbf{x}}, \hat{\mathbf{y}}, \hat{\mathbf{z}})$ system used by *Bieber et al.* [1996]; *Belcher and Davis* [1971] used the equivalent right-handed triad $(\hat{\mathbf{y}}, -\hat{\mathbf{x}}, \hat{\mathbf{z}})$. Thus $P_{zz}(\nu)$ is the power spectrum of fluctuations parallel to $\mathbf{B}_0 \equiv \langle \mathbf{B} \rangle$. Bieber et al. call $P_{xx}(\nu)$ the "quasi-parallel spectrum" $P_{(\parallel)}(\nu)$ because the fluctuation component under consideration (x) has a component parallel to the sampling direction; similarly, they denote $P_{yy}(\nu)$ as the "perpendicular" spectrum $P_{(\perp)}(\nu)$ because the y component is perpendicular to the (radial) sampling direction. The Bieber et al. terminology is based upon standard turbulence nomenclature [e.g., *Batchelor*, 1953]. The total spectrum for fluctuations perpendicular to the mean magnetic field as discussed in section 2.3 is

$$
\begin{aligned}
P_\perp(\nu) &= P_{(\parallel)}(\nu) + P_{(\perp)}(\nu) \\
&= P_{xx}(\nu) + P_{yy}(\nu).
\end{aligned}
$$

4.1. Slab and 2-D Fluctuations

In order to conduct our ratio test of turbulence geometry, we first assume a two-component model, which is a composite of slab and 2-D geometries. Although the results of sections 2–3 allow for the possibility of oblique wave vectors at other than $0°$ and $90°$ relative to $\mathbf{B}_0$, we will adopt this limitation for the purpose of demonstration. The existence of a significant 2-D component was first put forward by *Matthaeus et al.* [1990] and has subsequently been supported by *Zank and Matthaeus* [1992a] and *Bieber et al.* [1994, 1996]. See also the review by *Matthaeus et al.* [1995].

Again following the notation of *Bieber et al.* [1996], C_S and C_2 are the amplitudes of the slab and 2-D components, respectively; that is, the slab spectrum in the range of interest is parameterized by $C_S \nu^{-q}$.

The "slab fraction" r is the contribution of the slab component to the energy spectrum, relative to the total energy:

$$r \equiv \frac{C_S}{C_S + C_2} = \frac{1}{1 + r'}, \qquad (8)$$

where $r' = C_2/C_S$. We assume that both P_{xx} and P_{yy} obey the same power law (that is, they have the same spectral index $-q$). This is not strictly obeyed, at least not within our data set, but is approximately true with the notable exception mentioned in section 2. Equations (16) and (17) of *Bieber et al.* [1996] and the above definitions and assumptions leads us to the following formula for the ratio of power between components:

$$
\begin{aligned}
\frac{P_{yy}(\nu)}{P_{xx}(\nu)} &= \frac{P_{(\perp)}(\nu)}{P_{(\parallel)}(\nu)} \\
&= \frac{C_S k_S^{1-q} + C_2 \left(\frac{2q}{1+q}\right) k_2^{1-q}}{C_S k_S^{1-q} + C_2 \left(\frac{2}{1+q}\right) k_2^{1-q}} \\
&= \frac{k_S^{1-q} + r' \left(\frac{2q}{1+q}\right) k_2^{1-q}}{k_S^{1-q} + r' \left(\frac{2}{1+q}\right) k_2^{1-q}} \qquad (9)
\end{aligned}
$$

where

$$
\begin{aligned}
k_S &\equiv \frac{2\pi\nu}{V_{SW}\cos\theta} \\
k_2 &\equiv \frac{2\pi\nu}{V_{SW}\sin\theta}.
\end{aligned}
$$

The ratio P_{yy}/P_{xx} (which under our assumptions becomes independent of frequency in the relevant range) and the parameters V_{SW}, $\theta = \Theta_{BV_{SW}}$, and q are derivable from observations by a single spacecraft. Thus the only unknown in (9) is r', which, in turn, gives us the slab fraction r.

For both slab and 2-D models, there is no power in the parallel fluctuations and $P_{zz}(\nu) = 0$. Furthermore, for pure slab turbulence ($r = 1$; $r' = 0$), axisymmetry leads to equality of P_{xx} and P_{yy} [*Bieber et al.*, 1996]. A pure 2-D geometry predicts that the ratio $P_{yy}(\nu)/P_{xx}(\nu)$ be equal to the power law index q. Equation (9) also gives the dependence on field-to-flow angle θ: as $\theta \to 0°$, $P_{yy}/P_{xx} \to 1$, and as $\theta \to 90°$, $P_{yy}/P_{xx} \to q$.

Although there may be a frequency dependence as the spectrum delves more deeply into the dissipation range, we make the simplifying assumption that there is no frequency dependence for r or r' within the relevant range. For each interval we obtain one ratio P_{yy}/P_{xx} by averaging the ratio $P_{yy}(\nu)/P_{xx}(\nu)$ for
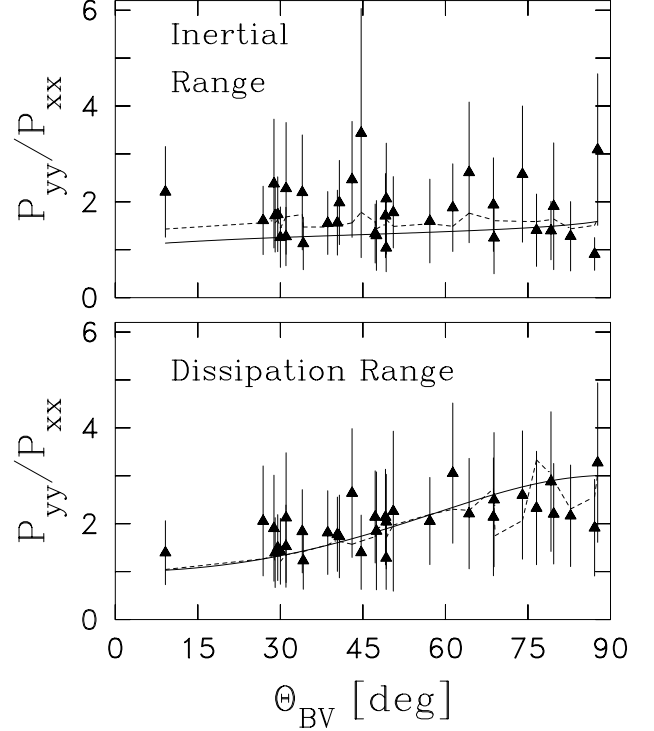

Figure 9. Ratio of perpendicular to parallel component spectra as a function of field-to-flow angle. (top) For the inertial range the best-fit curve is for $r = 0.11$ (11% slab component); (bottom) for the dissipation range, $r = 0.46$. Dashed curves show the best fit using individual observed power law indices, while the solid curves show the prediction of the best fit ratio using constant indices.

each frequency ν, excluding those frequencies within a $\pm10\%$ guard band of any harmonic of the spacecraft spin tone. An error bar was determined from the variance of the data.

We computed a P_{yy}/P_{xx} ratio for the same frequency ranges used to compute the spectral slopes of the high-frequency extent of the inertial range and the dissipation range, as discussed in section 2. These frequency ranges were not the same for each interval (they depend on the break frequency of the spectrum) but typically were ~0.01 to ~0.3 Hz for the inertial range and $\lesssim1$ to $\lesssim2$ Hz for the dissipation range.

4.2. Results

The results of P_{yy}/P_{xx} as a function of field-to-flow angle are shown in Figure 9. The curves shown are minimum χ^2 values of r, taking the spectral slopes to

be constant (1.66 for the inertial range and 3.04 for the dissipation range, which are the average spectral slopes for our data). However, the χ^2 statistic of the data set was computed using the observed value of q for each data point.

For the high-frequency inertial range described above, the minimum χ^2 of 10.87 occurs at $r = 0.11^{+0.20}_{-0.11}$. The indicated error bounds were determined from the values of r for which $\chi^2(r) = \chi^2_{\min} + 1$ [*Bevington*, 1969]. Note that the error bounds include $r = 0$, or a pure 2-D geometry; in fact, $\chi^2(r = 0) = 11.28$, which is still an acceptable fit. Despite the large error bars on the data points, we have 32 degrees of freedom, which implies that $r = 0.11$ is a good fit to the data. Taking the other limit, $\chi^2(r = 1) = 23.67$, which is almost low enough to be acceptable.

For the dissipation range the minimum χ^2 of 7.31 occurs at $r = 0.46^{+0.13}_{-0.11}$. This is a good fit, whereas $\chi^2(r = 0) = 106.0$ and $\chi^2(r = 1) = 30.72$ are not. The best fit value of $r = 0.46$ indicates that the slab fraction is increased in the dissipation range relative to the inertial range. There is a higher percentage of energy that resides in wave vectors aligned with the magnetic field in the dissipation range than in the inertial range.

5. Dynamical Description Possibilities

As discussed in section 3, the observed data cannot solely be explained by parallel-propagating waves. From an entirely different perspective the examination of the data in section 4 suggests that a substantial fraction of the magnetic fluctuation energy in the dissipation range resides in highly oblique Fourier modes. The latter procedure is entirely of a geometric nature and is completely unbiased with regard to the dynamical nature of the excitations associated with the oblique wave vectors. (Note, however, that conversion from frequency to wave vector using a single spacecraft requires use of the "frozen-in assumption," which requires that the characteristic speed of the fluctuations, e.g., wavelength over dynamical timescale, be much smaller than the solar wind speed.) In any event, there remains the challenge of finding a dynamical model that might adequately describe these highly transverse, nonslab fluctuations, thus forming a physical basis for understanding the couplings that connect fluid and kinetic scales in the dissipation range. Of the various possibilities for such a dynamical model, two well-studied examples are obliquely propagating waves and 2-D MHD turbulence.

5.1. Obliquely Propagating Waves

Consider the possibility that obliquely propagating waves form at least a portion of the inferred 2-D component. As is well understood, there are three wave modes for low-frequency, obliquely propagating electromagnetic waves: (1) the fast magnetosonic wave, (2) the shear Alfvén wave, and (3) the slow-mode wave.

Both the fast magnetosonic wave and the slow-mode wave are heavily damped in a high-β plasma, regardless of wavelength [*Barnes*, 1979]. However, observations reported here and elsewhere indicate the presence of a spectral breakpoint at scales near those of ion gyromotion, which we associate here with the dissipation processes. In this interpretation it is highly unlikely that the fast- and slow-mode waves can provide an adequate explanation of the observed data. The shear Alfvén wave has a dispersion relation $\omega = k_\parallel v_A$ for small values of k and is not damped in this regime. However, when the wavenumber k increases such that $k_\perp \rho_p \sim 1$, where ρ_p is the proton Larmor radius, the shear Alfvén wave becomes the kinetic Alfvén wave [*Hasegawa and Sato*, 1989; *Stix*, 1992], and it develops a substantial parallel electric field component. In this regime the kinetic Alfvén wave is highly dispersive, and the real part of the wave frequency asymptotically approaches the ion cyclotron frequency. Electron Landau damping becomes important because of the presence of the parallel electric field component, and ion cyclotron damping can also play a significant role in the damping process if $\omega_r \sim \Omega_p$.

It is clear that if some of the fluctuations are kinetic Alfvén waves, dissipation should occur when $k_\perp \rho_p \sim 1$ or $k v_A / \Omega_p \sim 1$. The dissipation scale length associated with kinetic Alfvén waves is quite consistent with the observed dissipation range; thus it is possible that part of the observed fluctuation spectrum can be attributed to kinetic Alfvén waves and the damping of these waves can give rise to the dissipation range.

The advantages of an explanation based upon kinetic Alfvén waves are that (1) they possess wave vectors at large angles to the mean magnetic field, which is in general agreement with the conclusions of sections 2–4, (2) they provide both cyclotron resonant dissipation and dissipation via the generation of parallel electric fields at comparable wavenumbers, and (3) the two distinct mechanisms provide separate, coincident mechanisms for heating both background ions and electrons. The theory of kinetic Alfvén wave damping is not alone in this regard, but the theory is significantly more advanced than the related option

that follows.

5.2. Two-Dimensional MHD Turbulence

An alternative dynamical model for dissipation range fluctuations is that they consist of two components: (1) slab waves with wave vectors along (or nearly along) the mean field and (2) 2-D MHD turbulence, having wave vectors nearly perpendicular to the mean field. Unlike the kinetic wave description, this dynamical model does not lend itself to a compact representation based upon eigenmodes and dispersion relations. However, the dynamics of 2-D turbulence has been widely studied using statistical theories and simulations [e.g., *Kraichnan and Montgomery*, 1980; *Matthaeus and Montgomery*, 1980; *Matthaeus and Lamkin*, 1986]. The slab/2-D composite model also emerges as a natural description of anisotropic plasma turbulence in the reduced MHD regime [*Montgomery*, 1982] and can be seen to emerge as a consequence of a formal treatment of nearly incompressible MHD at low and order-one β_p [*Zank and Matthaeus*, 1993]. The two component model also has found use in various solar wind applications (see review by *Matthaeus et al.* [1995]), including transport of turbulence [*Tu and Marsch*, 1993] and cosmic ray scattering [*Bieber et al.*, 1994].

As far as we are aware, most previous studies that employ a two component turbulence representation (or, its close relatives, quasi-2-D or reduced MHD models) have not attempted to characterize magnetofluid or kinetic plasma dynamics in the dissipation range in any detail. However, it is clear that such a model presents interesting possibilities for influencing the dissipation range. For example, in a reduced MHD or two-component model [*Montgomery*, 1982; *Zank and Matthaeus*, 1992b; R. Kinney and J.C. McWilliams, Turbulent cascades in anisotropic magnetohydrodynamics, submitted to Phys. Rev. E, 1997] the 2-D fluctuations are expected to engage most vigorously in the cascade phenomena that transfer excitations through the inertial range and into the smaller dissipation scales. Thus established MHD effects are capable of supplying the dissipation range with a flux of energy from the substantial reservoirs typically found at the large scales. This dissipation, in models with simplified transport coefficients [e.g., *Matthaeus and Lamkin*, 1986], is expected to occur near X-type neutral points in the poloidal field through processes related to magnetic reconnection.

A second relevant feature of models with a significant admixture of 2-D turbulence relates directly to the potential for dynamical couplings with kinetic processes. In particular, it has been estab-

lished through studies of test particle orbits in dynamical MHD fields [*Ambrosiano et al.*, 1988; *Gray and Matthaeus*, 1992] that 2-D turbulence can account for substantial amounts of charged particle acceleration. Typically, a broad spectrum of energetic particles is formed, and for turbulence with energy-containing scale L, test particle energies can range up to values of $\Omega_p L/v_A$ times their initial low values (e.g., initial particle speed v_A). The process by which this occurs is complex [*Ambrosiano et al.*, 1988] and appears to involve temporary trapping of test particles in or near small scale fluctuations that form near reconnection zones near magnetic X points. A full analytical theory of this acceleration process has not yet been developed, but it seems plausible that MHD structures with transverse scales of the order of the thermal particle gyroradius might be involved. The matching conditions associated with efficient acceleration of this type are most likely temporal resonance conditions but in any case cannot involve the usual spatial resonance condition (equation (5)), since such couplings are absent for 2-D MHD fluctuations having $k_{\parallel} = 0$. The scenario in which MHD energy flows into particle energy can only be suggested by test particle studies. A full kinetic treatment is required to demonstrate the feasibility of the above process as a means of coupling MHD scales to kinetic scales and thereby forming a dissipation range. However, the existing test particle studies provide ample motivation to further examine this possibility.

The dynamical perspectives associated with the 2-D turbulence and kinetic Alfvén waves are quite different, but the two paradigms are not inconsistent either. Kinetic Alfvén wave theory takes into account couplings to the kinetic degrees of freedom of the plasma and ignores "wave-wave" couplings among the waves. The 2-D turbulence perspective takes full account of the couplings between the various MHD scale Fourier modes (analogous to wave-wave couplings) but discards the kinetic couplings. In this light, the two models are not contradictory but, rather, are complementary. In fact, from a geometrical or kinematic point of view the two models are nearly indistinguishable, and the nonslab, transverse magnetic fluctuations identified in section 4 might equally well display the dynamical features of either model.

An additional feature that is common in the two models and that is of particular interest from the point of view of dissipation mechanisms is the parallel electric field. For kinetic Alfvén waves the parallel electric field is an integral feature of the eigenmodes at cyclotron scales. For 2-D turbulence a parallel induced electric field is associated with $\delta \mathbf{V} \times \delta \mathbf{B}$ (where

$\delta\mathbf{V}$ and $\delta\mathbf{B}$ are the plasma velocity and magnetic field fluctuations, respectively). In both cases the parallel electric field would be expected to couple to kinetic processes, for example, in the manner described by *Wong et al.* [1997], presumably leading to heating of the plasma and dissipation of MHD scale energy in both cases.

6. Summary

We have undertaken to study and parameterize the dissipation range of IMF fluctuations and its causes. We have repeated the analyses of two inertial range studies [*Belcher and Davis*, 1971; *Bieber et al.*, 1996] and extended their results to include the dissipation range using the increased capabilities of the Wind spacecraft.

The results of our investigation of magnetic fluctuations agree for the most part with those of *Belcher and Davis* [1971]: the total variances transverse to and aligned with the mean field are in a ratio 10.4:1 for the high-frequency end of the inertial range. In the same coordinate system $(\hat{\mathbf{B}} \times \hat{\mathbf{R}}, \hat{\mathbf{B}} \times (\hat{\mathbf{B}} \times \hat{\mathbf{R}}), \hat{\mathbf{B}})$ used by Belcher and Davis the ratio of geometric mean variances is 6.7:3.7:1. In the dissipation range, transverse fluctuations are less dominant, and the ratio of total transverse to parallel powers falls to 4.9:1, while the component-to-component ratio becomes 3.3:1.6:1.

We also agree with the *Belcher and Davis* [1971] observation that temperature is correlated with spectral index. Hotter intervals tend to have shallower inertial ranges and steeper dissipation ranges. This suggests that hotter intervals tend to have greater heating rates due to the more rapid dissipation of magnetic energy.

The onset of the dissipation range, the spectral break frequency $\nu_{\rm bf}$, occurs at frequencies roughly comparable to the proton cyclotron frequency $\nu_{\rm pc}$. Together with a bias in the magnetic helicity spectrum that implies a depletion of outward propagating Alfvén waves, which is observed in all but six of the 33 events used in this study, one would expect resonant cyclotron damping to explain the dissipation range. However, we find that Doppler-shifted resonant damping cannot explain the observations, and the percentage errors tend to 100% as the field-to-flow angle $\Theta_{BV_{Sw}}$ becomes 90°. In fact, any imposed $\Theta_{BV_{Sw}}$ dependence leads to a systematic error in the results. This difficulty can be avoided by considering more general geometries of magnetic fluctuations.

Repeating the analyses of *Bieber et al.* [1996], we find that fluctuations in the high-frequency end of the inertial range are best described by a mixture of 11%

slab waves and 89% 2-D geometry with the greatest percentage of wave vectors at large angles to the mean magnetic field. In the dissipation range the fluctuations are best described by a mixture of 46% slab waves and 54% 2-D geometry. The increased slab fraction may be explained by the preferential dissipation of oblique structures. Whatever the mechanism of dissipation, it must leave a polarized magnetic helicity spectrum in the remaining slab fraction exactly as observed.

Our test of the dissipation range geometry does not indicate the nature or dynamics of the 2-D component. Although we have discussed it largely within the context of past turbulence discussions, it is possible that kinetic Alfvén waves may form some fraction of this turbulence. As such, the dissipation of kinetic Alfvén waves either by ion cyclotron damping or electron Landau damping may be significant to the formation of the dissipation range. Likewise, turbulent trapping of particles by closed-field structures and acceleration by parallel electric fields generated by the MHD turbulence may be significant.

It is also true that our geometry analysis requires the assumption that the fully 3-D spectrum be formed from slab and 2-D components. A general axisymmetric spectrum is not permitted. It is difficult to conclude how this analysis would respond to the situation of slab plus moderately oblique waves as suggested by *Sari and Valley* [1976]. The existence of nonzero spectral power for the component along the mean magnetic field continues to support the latter view, and it seems likely that the fully 3-D spectrum is a combination of slab, 2-D, and oblique wave vectors. This analysis suggests that the 2-D component dominates.

This paper began by discussing two paradigms for the IMF fluctuations and their implications for solar wind heating. While this work has not entirely ruled out the simpler paradigm of noninteracting waves, it has severely limited its applicability. It is now necessary that a significant fraction of the magnetic wave energy reside in highly oblique waves and that the onset of dissipation not be governed by the dynamics of ion cyclotron damping of parallel-propagating waves.

References

Ambrosiano, J., W. H. Matthaeus, M. L. Goldstein, and D. Plante, Test particle acceleration in turbulent reconnecting magnetic fields, *J. Geophys. Res., 93*, 14,383–14,400, 1988.

Barnes, A., Collisionless damping of hydromagnetic waves, *Phys. Fluids, 9*, 1483–1495, 1966.

Barnes, A., Hydromagnetic waves and turbulence in the solar wind, in *Solar System Plasma Physics*, Vol. 1, edited by E. N. Parker, C. F. Kennel, and L. J. Lanzerotti, pp. 249–319, North-Holland, New York, 1979.

Batchelor, G. K., *The Theory of Homogeneous Turbulence*, Cambridge Univ. Press, New York, 1953.

Behannon, K. W., Observations of the interplanetary magnetic field between 0.46 and 1 AU by the Mariner 10 spacecraft, Ph.D. thesis, Catholic Univ. of Am., Washington, D.C., 1975.

Belcher, J. W., and L. Davis Jr., Large-amplitude Alfvén waves in the interplanetary medium, 2, *J. Geophys. Res., 76*, 3533–3563, 1971.

Bevington, P. R., *Data Reduction and Error Analysis for the Physical Sciences*, McGraw-Hill, New York, 1969.

Bieber, J. W., J. Chen, W. H. Matthaeus, C. W. Smith, and M. A. Pomerantz, Long-term variations of interplanetary magnetic field spectra with implications for cosmic ray modulation, *J. Geophys. Res., 98*, 3585–3603, 1993.

Bieber, J. W., W. H. Matthaeus, C. W. Smith, W. Wanner, M.-B. Kallenrode, and G. Wibberenz, Proton and electron mean free paths: The Palmer consensus revisited, *Astrophys. J., 420*, 294–306, 1994.

Bieber, J. W., W. Wanner, and W. H. Matthaeus, Dominant two-dimensional solar wind turbulence with implications for cosmic ray transport, *J. Geophys. Res., 101*, 2511–2522, 1996.

Blackman, R. B., and J. W. Tukey, *The Measurement of Power Spectra*, Dover, Mineola, N.Y., 1958.

Chen, J., Long-term modulation of cosmic rays in interplanetary magnetic turbulence, Ph.D. thesis, Univ. of Del., Newark, 1989.

Chen, J., J. W. Bieber, and M. A. Pomerantz, Cosmic ray unidirectional latitude gradient: Evidence for north-south asymmetric solar modulation, *J. Geophys. Res., 96*, 11,569–11,585, 1991.

Coleman, P. J., Jr., Hydromagnetic waves in the interplanetary plasma, *Phys. Rev. Lett., 17*, 207–211, 1966.

Coleman, P. J., Jr., Turbulence, viscosity, and dissipation in the solar wind plasma, *Astrophys. J., 153*, 371–388,

1968.

Daily, W. D., Alfvén wave refraction by interplanetary inhomogeneities, *J. Geophys. Res., 78*, 2043–2053, 1973.

Denskat, K. U., H. J. Beinroth, and F. M. Neubauer, Interplanetary magnetic field power spectra with frequencies from 2.4×10^{-5} Hz to 470 Hz from Helios-observations during solar minimum conditions, *J. Geophys., 54*, 60–67, 1983.

Freeman, J. W., Estimates of solar wind heating inside 0.3 AU, *Geophys. Res. Lett., 15*, 88–91, 1988.

Goldstein, M. L., D. A. Roberts, and C. A. Fitch, Properties of the fluctuating magnetic helicity in the inertial and dissipation ranges of solar wind turbulence, *J. Geophys. Res., 99*, 11,519–11,538, 1994.

Goldstein, M. L., D. A. Roberts, and W. H. Matthaeus, Magnetohydrodynamic turbulence in the solar wind, *Annu. Rev. Astron. Astrophys., 33*, 283–325, 1995.

Gray, P. C., and W. H. Matthaeus, MHD turbulence, reconnection and test-particle acceleration, in *Particle Acceleration in Cosmic Plasmas*, edited by G. P. Zank and T. K. Gaisser, pp. 261–266, (Am. Inst. of Phys., College Park, Md.), 1992.

Hasegawa, A., and T. Sato, *Space Plasma Physics*, Vol. 1, *Stationary Processes*, Springer-Verlag, New York, 1989.

Hollweg, J. V., On WKB expansions for Alfvén waves in the solar wind, *J. Geophys. Res., 95*, 14,873–14,879, 1990.

Klein, L. W., D. A. Roberts, and M. L. Goldstein, Anisotropy and minimum variance directions of solar wind fluctuations in the outer heliosphere, *J. Geophys. Res., 96*, 3779–3788, 1991.

Kolmogoroff, A. N., The local structure of turbulence in incompressible viscous fluid for very large Reynolds numbers, *Dokl. Akad. Nauk SSSR, 30*, 301–305, 1941.

Kraichnan, R. H., and D. C. Montgomery, Two dimensional turbulence, *Rep. Prog. Phys., 43*, 547–619, 1980.

Lepping, R. P., et al., The Wind magnetic field investigation, *Space Sci. Rev., 71*, 207–229, 1995.

Marsch, E., Kinetic physics of the solar wind plasma, in *Physics of the Inner Heliosphere*, Vol. 2, *Particles, Waves and Turbulence*, edited by R. Schwenn and E. Marsch, pp. 45–133, Springer-Verlag, New York, 1991.

Matthaeus, W. H., and M. L. Goldstein, Measurement of the rugged invariants of magnetohydrodynamic turbulence in the solar wind, *J. Geophys. Res., 87*, 6011–6028, 1982.

Matthaeus, W. H., and S. L. Lamkin, Turbulent magnetic reconnection, *Phys. Fluids, 29*, 2513–2534, 1986.

Matthaeus, W. H., and D. C. Montgomery, Selective decay hypothesis at high mechanical and magnetic Reynolds numbers, in *Nonlinear Dynamics*, edited by R. H. G. Helleman, Ann. N. Y. Acad. Sci., *357*, 203–222, 1980.

Matthaeus, W. H., M. L. Goldstein, and D. A. Roberts, Evidence for the presence of quasi-two-dimensional nearly incompressible fluctuations in the solar wind,

J. Geophys. Res., 95, 20,673–20,683, 1990.

Matthaeus, W. H., J. W. Bieber, and G. P. Zank, Unquiet on any front: Anisotropic turbulence in the solar wind, *Rev. Geophys.*, U.S. Natl. Rep. Int. Union Geod. Geophys. 1991–1994, *33*, 609–614, 1995.

Moffatt, H. K., *Magnetic Field Generation in Electrically Conducting Fluids*, Cambridge Univ. Press, New York, 1978.

Montgomery, D. C., Major disruption, inverse cascades, and the Strauss equations, *Phys. Scr., T, 2*(1), 83–88, 1982.

Ogilvie, K. W., et al., SWE, A comprehensive plasma instrument for the Wind spacecraft, *Space Sci. Rev., 71*, 55–77, 1995.

Oughton, S., Transport of solar wind fluctuations: A turbulence approach, Ph.D. thesis, Univ. of Del., Newark, 1993.

Richardson, J. D., K. I. Paularena, A. J. Lazarus, and J. W. Belcher, Radial evolution of the solar wind from IMP 8 to Voyager 2, *Geophys. Res. Lett., 22*, 325–328, 1995.

Sari, J. W., and G. C. Valley, Interplanetary magnetic field power spectra: Mean field radial or perpendicular to radial, *J. Geophys. Res., 81*, 5489–5499, 1976.

Schwartz, S. J., W. C. Feldman, and S. P. Gary, The source of proton anisotropy in the high-speed solar wind, *J. Geophys. Res., 86*, 541–546, 1981.

Smith, C. W., M. L. Goldstein and W. H. Matthaeus, Turbulence analysis of the Jovian upstream "wave" phenomenon, *J. Geophys. Res., 88*, 5581–5593, 1983. (Correction, *J. Geophys. Res., 89*, 9159–9160, 1984.)

Smith, C. W., W. H. Matthaeus, and N. F. Ness, Measurement of the dissipation range spectrum of magnetic fluctuations in the solar wind with applications to the diffusion of cosmic rays, *Proc. Int. Conf. Cosmic Rays 21st*, (5), 280–283, 1990.

Stix, T. H., *Waves in Plasmas*, Am. Inst. of Phys., College Park, Md., 1992.

Tu, C.-Y., and E. Marsch, A model of solar wind fluctuations with two components: Alfvén waves and convective structures, *J. Geophys. Res., 98*, 1257–1276, 1993.

Tu, C.-Y., and E. Marsch, *MHD Structures, Waves and Turbulence in the Solar Wind*, Kluwer Acad., Norwell, Mass., 1995. (Reprinted from *Space Sci. Rev., 73*(1–2), 1995.)

Williams, L. L., and G. P. Zank, Effect of magnetic field geometry on the wave signature of the pickup of interstellar neutrals, *J. Geophys. Res., 99*, 19,229–19,244, 1994.

Wong, H. K., A. F. Viñas, and A. J. Klimas, Generation of high and low frequency waves by long-wavelength electric field fluctuations, *Eos, Trans. AGU, 78*(17), Spring Meet. Suppl., S251, 1997.

Zank, G. P., and W. H. Matthaeus, Waves and turbulence in the solar wind, *J. Geophys. Res., 97*, 17,189–17,194, 1992a.

Zank, G. P., and W. H. Matthaeus, The equations of reduced magnetohydrodynamics, *J. Plasma Phys., 48*, 85–100, 1992b.

Zank, G. P., and W. H. Matthaeus, Nearly incompressible fluids, II, Magnetohydrodynamics, turbulence and waves, *Phys. Fluids A, 5*, 257–273, 1993.

Zank, G. P., W. H. Matthaeus, and C. W. Smith, Evolution of turbulent magnetic fluctuation power with heliospheric distance, *J. Geophys. Res., 101*, 17,093–17,107, 1996.

R.J. Leamon, W.H. Matthaeus, N.F. Ness, and C.W. Smith, Bartol Research Institute, University of Delaware, Newark, DE 19716. (e-mail: leamon@bartol.udel.edu; yswhm@bartol.udel.edu; nfness@bartol.udel.edu; chuck@bartol.udel.edu)

H.K. Wong, Aurora Science Inc., 4502 Centerview Drive, San Antonio, TX 87228. (e-mail: kit@cascade.gsfc.nasa.gov)